Experimental investigation of potential topological and p-wave superconductors

Trần, V.B.

Publication date
2014

Chapter 3 Theoretical aspects

This chapter summaries theoretical aspects of the research themes presented throughout the PhD work. We start with a general description of quantum criticality and quantum phase transitions. Then the focus is directed towards superconductivity, especially to the novel class of ferromagnetic superconductors with the case study UCoGe. Next, a brief overview is presented of a new research field in condensed matter physics: topological insulators and topological superconductors. Subsequently, we discuss superconductivity in a magnetic field. In particular, we consider the upper critical field for both conventional BCS s-wave and unconventional superconductors. These theoretical aspects will be applied in the case studies of the doped topological insulator $Cu_xBi_2Se_3$ and the noncentrosymmetric superconductor YPtBi.

3.1 Ferromagnetic superconductors

3.1.1 Quantum criticality

Phase transitions are not only simply ubiquitous in nature but also play a crucial role in shaping the world. Macroscopically, phase transitions in the universe form galaxies, stars and planets. Phase transitions in our daily life are the transformation of for instance water between ice, liquid and vapor. These phase transitions are called thermal or classical and are controlled by thermal fluctuations. Therefore, in the classical world, matter in equilibrium freezes at absolute zero temperature in order to minimize the potential energy.

Quantum mechanics, however, allows fluctuations even at zero temperature. Once such quantum fluctuations are sufficiently strong, the system undergoes a quantum phase transition as illustrated in Fig. 3.1 [1]. Quantum phase transitions (QPTs) are driven by a non-thermal parameter *r*, such as pressure, magnetic field, chemical doping or electron density. By changing the control parameters one is able to tune the system to a transition point, the quantum critical point (QCP).

A continuous phase transition can usually be described by an order parameter, a concept first introduced by Landau. This parameter is a thermodynamic quantity that depends on the state of the system. Its thermodynamic average is equal to zero in the disordered phase

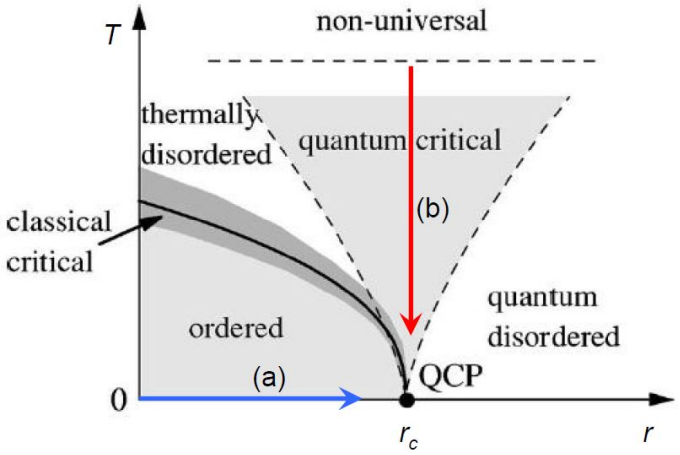

Figure 3.1 Global phase diagram of continuous phase transitions. *r* depicts the non-thermal control parameter, and *T* is the temperature. The solid line separates ordered and disordered regions, and ends at the QCP. The shadowed region close to this boundary implies the critical state is classical. The area bounded by the dashed lines given by $k_B T \propto |r - r_c|^{\nu z}$ indicates the quantum critical region. On the right of this region is the quantum disordered phase. The system can be tuned to the QCP by means of either changing $r \rightarrow r_c$ at $T = 0$ (a) or driving $T \rightarrow 0$ at $r = r_c$ (b) (picture taken from [1]).

and to non-zero in the ordered phase, *e.g.* the ordered moment M for ferromagnetism or the energy gap of a superconductor. Furthermore, the correlation length ξ of the system, that expresses the spatial range of correlation of the order parameter, turns out to be long-ranged when approaching the phase transition or the critical point. Notably, close to the QCP, the correlation length diverges, as a power law

$$\xi \propto t^{-\nu}, \tag{3.1}$$

where ν is the correlation length critical exponent, and t represents some dimensionless distance from the critical point. It can be defined by $t = |T\text{-}T_c|/T_c$ for the classical phase transitions at non-zero temperature T_c or by $t = |r\text{-}r_c|/r_c$ for QPTs.

Analogous to the length scale, the correlations of the order parameter fluctuations in time can be defined as τ_c, which is the typical time scale for the decay of the fluctuations due to a perturbation

$$\tau_c \propto \xi^z \propto t^{-\nu z}, \tag{3.2}$$

where z is the dynamical critical exponent. In addition, a critical frequency ω_c is defined by $1/\tau_c$. At the classical critical point, $\omega_c \rightarrow 0$ or the typical energy scale becomes zero, and this is called critical slowing down

$$\omega_c(t \rightarrow 0) \propto 1/\tau_c \rightarrow 0. \tag{3.3}$$

It is worth to notice that for the classical case, the kinetic and potential energy operators do not commute. This implies the dynamics and statistics are decoupled while, in contrast, for the quantum phase transition they are coupled [1].

In order to clarify the importance of quantum fluctuations at very small but non-zero T, one should take into account two typical energy scales: $\hbar\omega$ and k_BT. The quantum fluctuations remain dominant down to very low T as long as $\hbar\omega \gg k_BT$. As depicted by arrows in Fig. 3.1, quantum criticality can be studied both theoretically and experimentally by not only varying the control parameter r at $T = 0$ but also by lowering the temperature T at r_c.

Heavy fermion systems are model systems in which to investigate QPTs. In these systems, the Kondo effect, that quenches the local moment of the *f*-electrons by conduction electron screening, competes with the Ruderman-Kittel-Kasuya-Yosida (RKKY) interaction, which favours long-range magnetic order. This competition results in an unmatched tunability of magnetic phase transitions [2–5]. Changing the non-thermal control parameter r, such as the magnetic field [6–10], pressure [11–14] or chemical doping [15–20], suppresses the magnetic ordering and concurrently tunes the system to the QPT at the QCP $r = r_c$.

3.1.2 Ferromagnetic superconductors

Superconductivity was discovered in a remarkable experiment carried out in 1911 by Heike Kamerlingh Onnes in Leiden [21]. More than 40 years later, the microscopic theory by Bardeen, Cooper and Schrieffer (BCS) successfully explained the origin of this fascinating phenomenon in most superconducting materials [22]. The fingerprint of this theory is the existence of Cooper pairs. A Cooper pair is a bound state of two electrons which is formed near the Fermi level by an attractive interaction mediated by lattice vibrations. The symmetry of the Cooper pairs can be classified by the total spin S and the total angular momentum L. In general, a two-electron system can have spin S = 0 or 1, and L = 0, 1, 2, 3,… Since the electrons are fermions, the total wave function of the Cooper pair state, which consists of a product of spatial and spin components, must be anti-symmetric under the exchange of particles due to the Pauli exclusion principle. This results in even spatial and odd spin functions or vice versa. Therefore, one can distinguish superconductors with the spin-singlet state (S = 0)

$$\phi_{ss} = \frac{1}{\sqrt{2}}\left(\left|\uparrow\downarrow\right\rangle - \left|\downarrow\uparrow\right\rangle\right) \tag{3.4}$$

e.g. s-wave (S = 0, L = 0) and *d*-wave (S = 0, L = 2), and with the spin-triplet state (S = 1)

$$\phi_{st} = \begin{cases} \left|\uparrow\uparrow\right\rangle \\ \frac{1}{\sqrt{2}}\left(\left|\uparrow\downarrow\right\rangle + \left|\downarrow\uparrow\right\rangle\right) \\ \left|\downarrow\downarrow\right\rangle \end{cases} \tag{3.5}$$

e.g. p-wave (S = 1, L = 1) and *f*-wave (S = 1, L = 3). Here $\left|\uparrow\uparrow\right\rangle$ and $\left|\downarrow\downarrow\right\rangle$ are called the equal-spin pairing (ESP) states.

The superconducting state with S = 0, L = 0 (*s*-wave) is fully explained by the standard BCS theory, and therefore called conventional. However, with the experimental discovery of certain classes of superconductors which go beyond the understanding of the standard BCS scenario, the field of unconventional superconductivity begun. These materials with condensates made up of lower symmetry Cooper pairs (*d*-wave, *p*-wave,…) are non *s*-wave superconductors. Unconventional superconductivity has been found in numerous materials over the last forty years. The prime example is ^{3}He [23,24], and later on heavy fermion SCs (see for instance [25–33]) and high temperature superconductors (cuprates [34,35] and iron pnictides [36,37]) were discovered.

According to the BCS theory, SC is incompatible with ferromagnetic order, while under special conditions it may coexist with antiferromagnetism. However, around 1980, it

was theoretically predicted that SC with ESP states could exist in itinerant ferromagnets (*p*-wave SC) [38] close to a FM QCP. Here the exchange of longitudinal spin fluctuations is proposed to mediate superconductivity. Twenty years later, the first ferromagnetic superconductor UGe_2 was discovered [30,39]. Subsequently, three more FMSCs URhGe [31,40], UIr [41–43] and UCoGe [44–46] were found. To date, a comprehensive, quantitative theory to fully resolve the superconducting pairing issue in FMSCs is not at hand.

In order to offer a qualitative interpretation for the coexistence of FM and SC near a FM QCP, spin fluctuation models have been used [38]. Within these models, the magnetic state can be understood in terms of an exchange interaction $\bar{I}$ and a Stoner enhancement factor $S = (1-\bar{I})^{-1}$. For the critical value $\bar{I} = 1$, a second-order quantum phase transition emerges, and the system transforms from the paramagnetic phase ($\bar{I} < 1$) to the ferromagnetic ($\bar{I} > 1$) phase (Fig. 3.2a). Notably, in the ferromagnetic regime, *p*-wave SC with ESP states is possible with different T_c's for the spin up ($|\uparrow\uparrow\rangle$) and spin down ($|\downarrow\downarrow\rangle$) states. This implies two superconducting phases can be present [38,47,48]. However, the emergence of these two superconducting phases depends sensitively on the details of the band structure. A pictorial of the coexistence of SC and magnetism in the spin-fluctuation model is given in Fig. 3.2b [49]. In contrast to the model prediction, SC was not observed in the PM phase in the cases of UGe_2 and UIr. A possible explanation is that ferromagnetic spin waves (magnons) couple to the longitudinal magnetic susceptibility which results in an enhancement of T_c in the FM phase [49,50]. A comprehensive treatment has been made by Roussev and Millis [50] where SC coexists with FM, leading to a superconducting dome and nonzero T_c at the QCP, as illustrated in Fig. 3.2c.

In UCoGe, muon spin rotation/relaxation (μSR) [51], nuclear magnetic resonance (NMR) and nuclear quadrupole resonance (NQR) [52,53] measurements provide unambiguous evidence that SC is driven by ferromagnetic spin fluctuations and that SC and FM coexist microscopically. The pairing mechanism for *p*-wave SC understood in terms of spin fluctuations is qualitatively illustrated in Fig. 3.3 (left) [54], where it is energetically favorable for two electrons to share the same polarization cloud. Approaching the QCP, however, the experimental phase diagram [46] of UCoGe deviates from the theory by Fay and Appel [38]. Upon increasing the external pressure, FM is depressed and disappears at p_c, while, most surprisingly, SC is enhanced, and even exists in the PM phase, unlike in other FMSCs. At $p > p_c$ SC is depressed. In fact, the unconventional superconducting state in the ferromagnetic phase of UCoGe can be considered as an analogue of the superfluid non-unitary phase A_2 of ^{3}He in a magnetic field [55]. A symmetry group analysis for triplet

superconducting order parameters using two band SC [56,57] explains the experimental temperature (T)- pressure (p) phase diagram of UCoGe, Fig. 3.3-right.

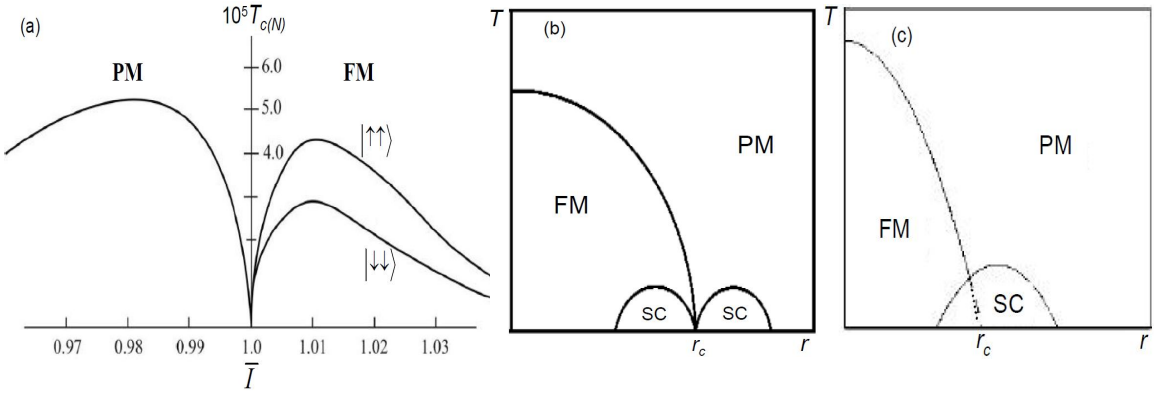

Figure 3.2 (a): Generic phase diagram of a p-wave SC. The superconducting transition temperature $T_{c(N)}$ as a function of the Stoner parameter $\bar{I}$ in the paramagnetic (PM) phase and the ferromagnetic (FM) phase. $T_{c(N)}$ is normalized by the Fermi temperature T_F. $|\uparrow\uparrow\rangle$ and $|\downarrow\downarrow\rangle$ in the FM phase indicate the ESP components (adapted from [38]). (b): Temperature (T) - control parameter (r) phase diagram of a FMSC according to the model given in [38]. SC emerges in both FM and PM phases centered around the QCP at r_c. To date, the SC dome in the PM phase has not been experimentally observed (adapted from [49]). (c): Temperature (T) - control parameter (r) phase diagram of a FMSC, where superconducting transition temperature T_c is finite at the QCP at r_c, and superconductivity coexists with ferromagnetism (adapted from [50]).

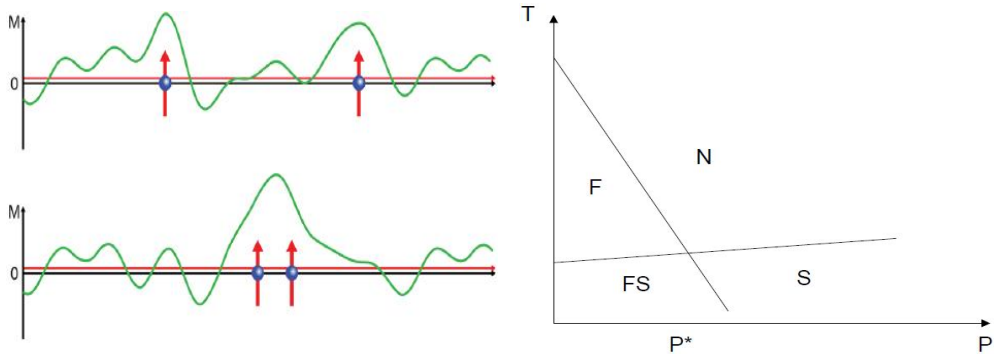

Figure 3.3 Left: Cartoon of electron pairing due to magnetic fluctuations. Non-zero average of the magnetization (upper, red horizontal lines in both frames) with a large fluctuating part. A local polarization cloud is created surrounding the electrons. For paired electrons (lower frame), the energy is lower than separate electrons (upper frame) (taken from [54]). Right: Generic temperature (T) - pressure (p) phase diagram of the FMSC UCoGe. SC is present in both the ferromagnetic (FS) and normal paramagnetic (S) phase. N and F depict the normal and ferromagnetic phase, respectively. Ferromagnetic order is not observed for pressure $p > p^*$ (adapted from [56]).

3.2 Topological insulators and superconductors

3.2.1 Topological insulators

TIs have emerged in condensed matter physics over the last few years as a completely new paradigm for research into novel phases of matter. This research field was theoretically predicted in 2005 [58] and the first TI was confirmed by experiment two years later [59]. Intriguing about TIs in contrast to ordinary bulk insulators is the existence of topologically non-trivial conducting surface states which are protected by time reversal symmetry (TRS). This means these surface states are in-sensitive to scattering from non-magnetic impurities.

In order to explain what a TI exactly is, it is first useful to consider one of the basic phenomena in condensed matter physics, the integer quantum Hall effect (IQHE). Consider a two dimensional system of classical electrons with charge *e* and mass *m* subjected to a perpendicular magnetic field *B*. In this case the charge carriers follow cyclotron orbits with the energy quantized in Landau levels

$$E_n = \hbar\omega_c(n+1/2), \tag{3.6}$$

where $\omega_c = eB/m$ is the cyclotron frequency, and $\hbar$ is Planck's constant. For a sufficiently large magnetic field, each Landau level is highly degenerate and the free electrons of the system occupy a few Landau levels only. This is the IQHE. In this regime the current flows along the edges of the sample, and the Hall conductivity is quantized

$$\sigma_{xy} = ne^2/h. \tag{3.7}$$

Here the filling factor *n* is a positive integer, and *n* turns out to be what is known as a Chern number: a topological invariant. Therefore, an IQH system possesses gapless edge states crossing the Fermi level while the bulk is insulating.

The main difference between an IQH system and an ordinary insulator is a matter of topology. According to the band structure point of view, the Bloch Hamiltonians of two given systems are topologically equivalent as long as they can be deformed continuously into each other, *i.e.* without closing the energy gap [60]. The Hamiltonian of an IQH insulator and that of a classical insulator belong to different topology classes. A topology class is generally defined by a topological invariant. For an IQH state, the topological invariant is the Chern number *n*, that remains unchanged as the Hamiltonian varies smoothly. The Chern number is related to an important quantity, the Berry phase, or geometric phase. The Berry phase is a phase difference in k-space of the wave function of a system when it is subjected to a cyclic adiabatic process [61,62]. The Berry phase is zero for ordinary insulators and an integer times π for TIs [60].

Quantum spin Hall effect (QSHE) is another example of a topological phase. In contrast to IQHE, in the quantum spin Hall effect, no magnetic field is required. The spin-orbit coupling of the band structure in the QSHE takes over the role of the magnetic field in the charge Hall effect. Again, the system possesses robust edge states that have a quantized spin-Hall conductance $\sigma_s = 2(e/4\pi)$. Here the charge conductance vanishes due to two equal currents flowing in opposite directions. Each conductivity channel contains its own independent Chern number $n_\uparrow$ or $n_\downarrow$, therefore the total Chern invariant for the Hall conductivity $n = n_\uparrow + n_\downarrow = 0$. In this case the Chern invariant cannot be used to classify the QSH state. Instead, a different topological invariant of the $\mathbb{Z}_2$ type ν, which is 0 or 1 [58], takes a value of 1 for the QSHE indicative of the topological character. Because of spin-orbit coupling the surface or edge states provide a net spin transport. The surface states have a Dirac-like dispersion and are topologically protected. This system is an example of a real 2D TI [59,60], see Fig. 3.4 for an illustration.

Furthermore, identification whether a system is topologically trivial or non-trivial is based on Kramer's theorem. As consequence of TRS for all spin 1/2 systems Kramer's theorem states that the eigenstates of a TR invariant Hamiltonian are at least twofold degenerate at time invariant points in *k*-space. In case of a 1D Brillouin zone ($k \geq 0$), these points are $k_x = \Gamma_a \equiv 0$ and $k_x = \Gamma_b \equiv \pi / a$. The way the time invariant points are connected depends on the topology of the system [60]. When the connection is pairwise (Fig. 3.5 - left), one can tune the system in such a way that none of these edge states crosses the Fermi level. However, this is not the case for an odd number of states passing E_F (Fig 3.5 - right). As a result, the former system is topologically trivial, with $\nu = 0$, whereas the latter is topologically nontrivial, with $\nu = 1$.

Another consequence of Kramer's theorem in the context of the fully spin polarized edge states of a TI or QSHE system is the absence of backscattering, even for strong disorder. Fig 3.6 shows schematically how an electron with spin 1/2 in a QSH edge state scatters from a non-magnetic impurity [63]. Due to the presence of the impurity its spin must reverse by moving either clockwise (Fig. 3.6 - upper frame) or anticlockwise (Fig. 3.6 - lower frame) around the impurity. As a result, the phase difference of the spin wave function is 2π. Also, quantum mechanics tells us for spin 1/2 systems the wave function satisfies $\Phi(\theta + 2\pi) = -\Phi(\theta)$. Thus, these two backscattering paths interfere destructively, which allows perfect transmission, with respect to such scattering from non-magnetic impurities. If the edge states possess an even number of left-moving channels and an even number of right-

moving channels, an electron can be scattered from the left-movers to the right-movers without reversing its spin. In this manner, the interference is non-destructive and thus there exists dissipation. TRS will be broken and consequently the interference is no longer destructive if the impurity carries a magnetic moment. Therefore, in QSH systems and in 2D TIs the elastic backscattering is forbidden, and the surface states are thus described as being robust and topologically protected by TRS.

Hitherto, we have been discussing topological states protected by TRS, next we discuss why a system could possesses such special surface states. TIs originate from the effect of strong SOC, which can lead to what is known as band inversion. Fig. 3.7 shows an example of band inversion in the 3D TI Bi_2Se_3 [64]. Consider the atomic energy levels at the Gamma point near the Fermi level E_F. These are mainly dominated by the p orbitals of Bi ($6s^26p^3$) and Se ($4s^24p^4$). Three effects eventually take place. Firstly, the chemical bonding between the Bi and Se atoms hybridizes their energy states. This process lowers the Se energy levels and, in contrast, raises the states of Bi. Next, the crystal-field splitting is added. The p_z levels of the Bi and Se are split off from the corresponding p_x and p_y orbitals, and are close to E_F, while the $p_{x,y}$ levels remain degenerate. In the last step, the effect of SOC is taken into account. The SOC Hamiltonian describing the system is given by $H_{SOC} = \lambda \mathbf{L}.\mathbf{S}$, where **L** and **S** are the orbital and spin angular momentum operators, respectively, and λ is a SOC parameter. Only when λ is sufficiently strong, the two states nearest to E_F turn out to be inverted which thus alters the parity of the occupied valence levels (below E_F) as a whole. For TIs with an inversion center [60] this is sufficient to make the bulk band structure topologically non-trivial.

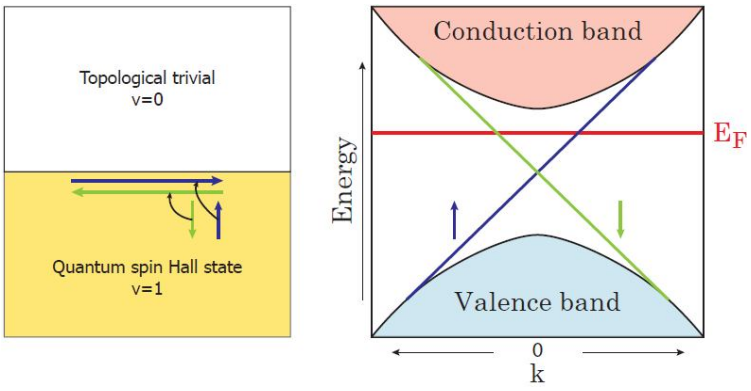

Figure 3.4 Left panel: A comparison between an ordinary insulator ($\nu = 0$) and the QSHE where the edge states are topologically nontrivial ($\nu = 1$). Right panel: the energy dispersion of the topologically nontrivial surface states (in the left panel) with up and down spins crossing the Fermi energy [60].

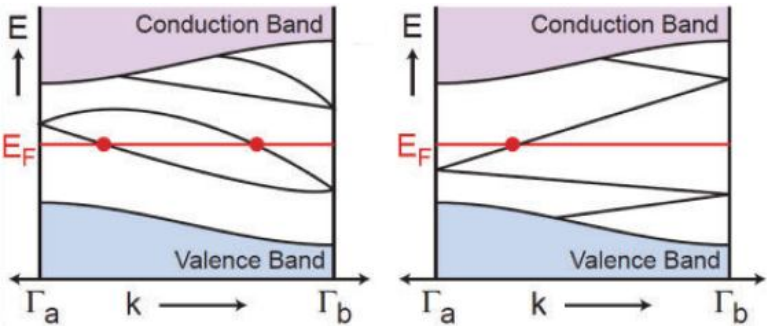

Figure 3.5 The electronic dispersions at two Kramers points Γ_a and Γ_b [60]. Left frame: Even number of states crossing the Fermi level results in topologically trivial states. Right frame: Topologically nontrivial states due to an odd number of states crossing the Fermi level.

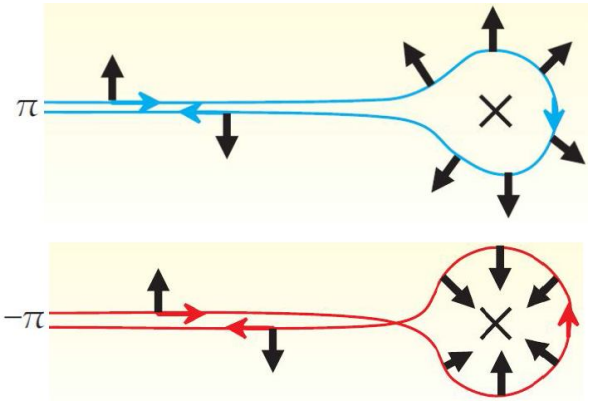

Figure 3.6 A scheme of a backscattering process taking place when an electron with spin 1/2 is subjected to a nonmagnetic impurity. Upper frame: spin rotates by π. Lower frame: spin rotates by $-\pi$. Adapted from [63].

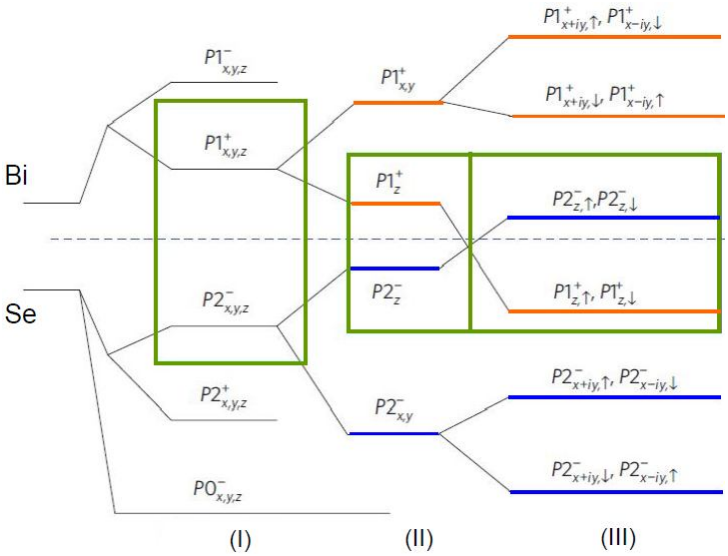

Figure 3.7 Energy levels of the 3D TI Bi_2Se_3 close to the E_F under the effects of chemical bonding (I), crystal field splitting (II) and SOC (III). The rightmost rectangle indicates the SOC, which leads to the band inversion. Picture taken from [64].

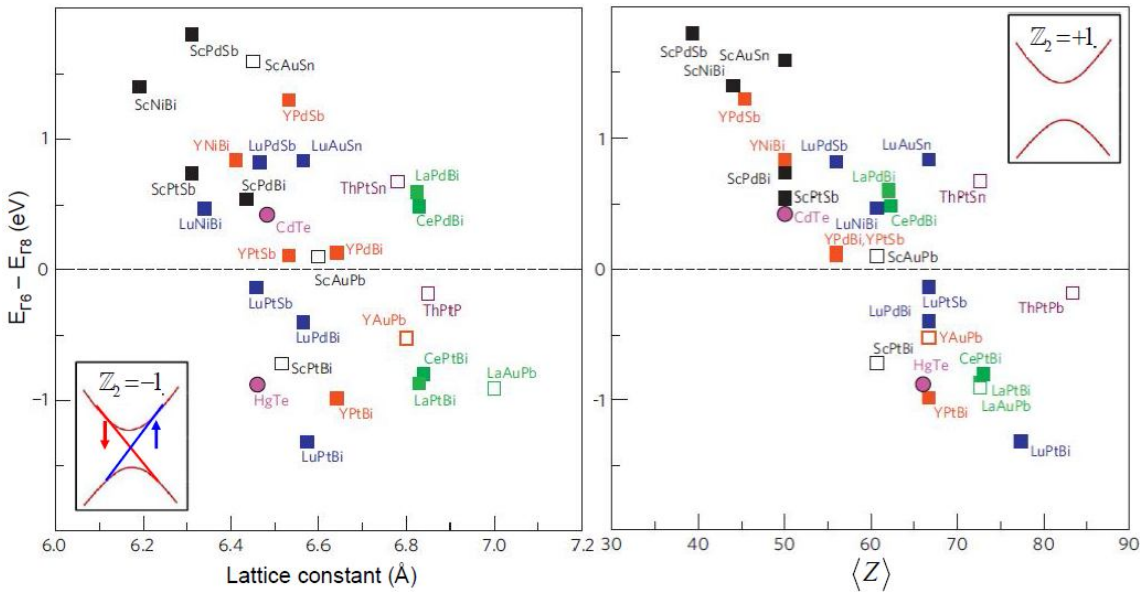

Figure 3.8 Band inversion of a number of Half-Heusler compounds as a function of the lattice constant and average nucleus charge $\langle Z \rangle$. There is a bulk bandgap between trivial states when the band inversion is absent (upper-right inset), and topologically nontrivial phases exist, providing protected edge states due to band inversion (lower-left inset) for the Half-Heusler systems. Adapted from [65].

Electronic structure calculations taking into account SOC and TRS show that several Half-Heusler compounds with a 111 stoichiometry also exhibit topological band inversion [65,66]. Fig. 3.8 shows that many systems are predicted to have a 'negative gap'- *i.e.* band inversion straddling around E_F, and thus be topological materials. The great diversity of the systems that can form Half-Heusler compounds yields a rich hunting ground for new topological non-trivial phases. In the case of the 111 system the band inversion takes place between the twofold-degenerate *s*-like Γ_6 and fourfold-degenerate *p*-type Γ_8 energy states in these materials and depends strongly on both the lattice constant and the SOC strength represented by an average charge $\langle Z \rangle$ of the nuclei. Consequently, the systems can be either topologically non-trivial (with $\Gamma_6 - \Gamma_8 < 0$; negative energy gap) or topologically trivial (with $\Gamma_6 - \Gamma_8 > 0$; positive energy gap). Amongst these Half Heusler compounds, four bismuth-based materials are also found to exhibit SC: YPtBi [67,68] (chapter 5), LaPtBi [69,70], LuPtBi [71] and ErPdBi [72].

Having briefly discussed 2D (QSHE) and 3D TIs, we continue by introducing a general picture of how to classify TIs and TSCs by their symmetries. Upon the presence or

absence of time-reversal symmetry (Θ), particle-hole symmetry (Ξ) and sublattice or chiral symmetry ($\Pi = \Theta\Xi$), the topological classifications for TIs and TSCs whose dimensionalities, *d*, are up to 8 are summarized in Fig. 3.9 [60,73]. Together these three symmetries form ten symmetry classes depicted by the Altland-Zirnbauer (AZ) notation. The symmetries can take a value of 0 or ±1, which denotes the absence or presence of the symmetries in the system, respectively. The ±1 indicates the value of Θ^2 and Ξ^2. The topological classifications are denoted by 0, $\mathbb{Z}$ and $\mathbb{Z}_2$, where 0 indicates topological phases are absent. $\mathbb{Z}$ presents a corresponding topological invariant that can take any positive integer value like the Chern number in the IQHE, and $\mathbb{Z}_2$ indicates a corresponding topological invariant that can take a value of 0 or ±1 as in the topological insulators. In this figure, one can locate the systems discussed so far. For example, the 2D IQHE denoted by $\mathbb{Z}$ is given by the entry in the first row and column 2 without any symmetry. The first TI experimentally realized is the HgTe/CdTe quantum well [59], d = 2 and row 7. Systems presented in this PhD work are $Cu_xBi_2Se_3$ (d = 3, row 6) and YPtBi (d = 3, row 8) which will be extensively discussed in the following chapters.

Notation	Symmetry			Dimension							
AZ	Θ	Ξ	Π	1	2	3	4	5	6	7	8
A	0	0	0	0	Z	0	Z	0	Z	0	Z
AIII	0	0	1	Z	0	Z	0	Z	0	Z	0
AI	1	0	0	0	0	0	Z	0	Z_2	Z_2	Z
BDI	1	1	1	Z	0	0	0	Z	0	Z_2	Z_2
D	0	1	0	Z_2	Z	0	0	0	Z	0	Z_2
DIII	−1	1	1	Z_2	Z_2	Z	0	0	0	Z	0
AII	−1	0	0	0	Z_2	Z_2	Z	0	0	0	Z
CII	−1	−1	1	Z	0	Z_2	Z_2	Z	0	0	0
C	0	−1	0	0	Z	0	Z_2	Z_2	Z	0	0
CI	1	−1	1	0	0	Z	0	Z_2	Z_2	Z	0

Figure 3.9 Classifications of TIs and TSCs. The notation of Altland and Zirnbauer (AZ) is used to denote ten different symmetry classes. Depending on the presence or absence of the symmetries Θ, Ξ and Π (see text), TIs and TSCs are classified with regards to their dimension, AZ symmetry, whereby the entries 0, $\mathbb{Z}$, and $\mathbb{Z}_2$ label the topological classes. The entries with circles are explained in the text as being relevant to particular material realizations. Table adapted from [60].

3.2.2 Topological superconductors

3.2.2.1 Odd and even-parity superconductors

In general, the symmetry group G^{sym} of the normal phase of a crystalline SC is given by

$$G^{sym} = G_0 \times G_s \times T \times U(1), \tag{3.8}$$

where G_0, G_s, T, and $U(1)$ presents orbital rotation, spin rotation, time-reversal symmetry and gauge symmetry, respectively [74]. Generally speaking, in conventional SC, only $U(1)$ is broken when the system undergoes SC, while in case of unconventional SC, at least one of the other symmetries is broken as well. For instance, time reversal symmetry T is broken in the SC phase of the FMSC UCoGe [47] and the correlated metal Sr_2RuO_4 [75,76].

The superconducting pair wave function, which yields the energy gap function or order parameter, is comprised of a spatial part (in momentum space k) and a spin part, S. For even parity (total spin $S = 0$), the wave function is invariant under inversion symmetry, while, in contrast, the wave function changes sign for odd parity ($S = 1$). Based on the gap symmetry one can distinguish different SCs. For conventional *s*-wave SCs, the superconducting gap has the highest symmetry and is nearly isotropic (although in practice there may be some anisotropy in the k-dependence of the gap magnitude). For unconventional SCs, the gap function has a lower symmetry. In Fig 3.10 sketches are given of examples of various unconventional superconducting states whose wave functions are classified by the combinations of S_z (the z-spin component) and m (the angular orbital momentum) in the superfluid phase of ^{3}He [77–79]. They include the A_1 phase with $|S_z = 1, m = 1\rangle$, the ABM (Anderson-Brinkman-Morel) phase with $|S_z = 1, m = 1\rangle$ and $|S_z = -1, m = 1\rangle$ and the BW (Balian-Werthamer) phase with $|S_z = -1, m = 1\rangle$, $|S_z = 0, m = 0\rangle$ and $|S_z = 1, m = -1\rangle$. Consequently, the corresponding gap symmetries of these states can be realized as shown in Fig. 3.11. In addition, there are polar and planar states, which are equally weighted superpositions of the two states with $|S_z = -1, m = 1\rangle$ and $|S_z = 1, m = -1\rangle$, and the Scharnberg-Klemm (SK) state [80], which possesses a similar gap symmetry as in the ABM state.

In the following chapters, we investigate superconducting phases of several materials according to these classifications.

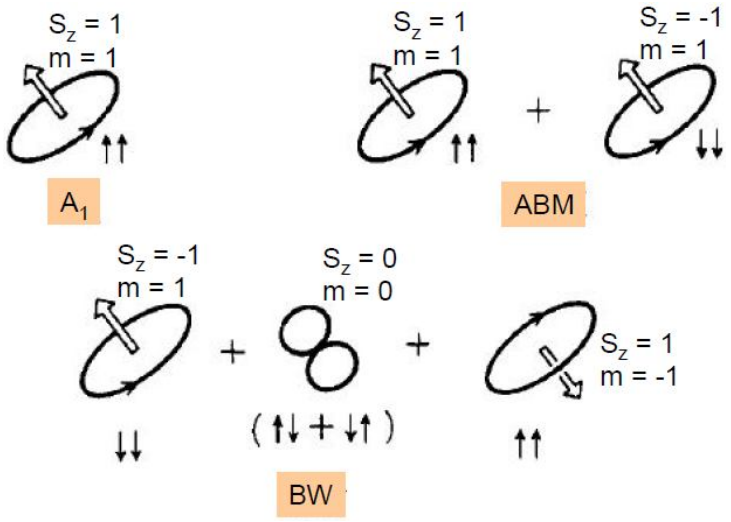

Figure 3.10 General scheme for the orbital and spin states in the superfluid phases A_1, ABM and BW of ^{3}He. Picture adapted from [79].

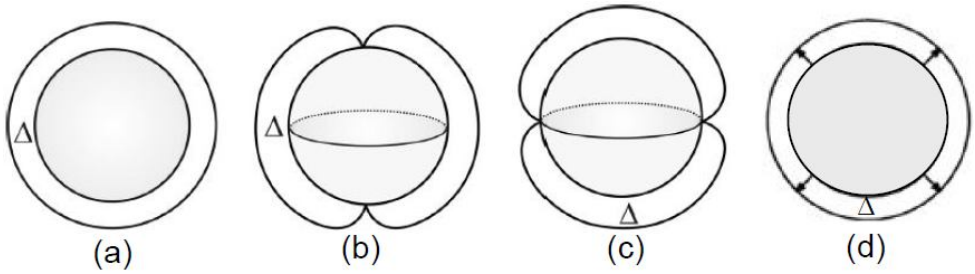

Figure 3.11 Superconducting energy gap at the Fermi surface for different states. (a) The isotropic gap of an *s*-wave superconductor. (b) The axial or point node gap as in the ABM state (the superfluid A phase of ^{3}He) where the gap terminates at two points (poles). (c) The polar (as in the planar-B phase of ^{3}He) state where the gap vanishes along a line on the Fermi surface. (d) Full gap (BW or as in the B phase) state of a *p*-wave superconductor.

3.2.2.2 Topological superconductors

Topological phases in superconductors have attracted ample attention even long before the birth of TIs. Topological superconductivity can be understood as a state that possesses a full superconducting gap in the bulk, but possesses topological edge states. The most well known candidate for TSC is superfluid ^{3}He (phase B) [77,78,81] described by the topological invariant $\mathbb{Z}$. Yet another promising test case for 2D chiral superconductivity is the triplet superconductor Sr_2RuO_4 [76], but experimental evidence remains under debate, for instance, as regards the existence of the gapless surface states [82]. Other candidate topological superconductors can be found among the doped TI $Cu_xBi_2Se_3$ [83,84], the half-Heusler 111

platinum bismuthides LaPtBi, YPtBi, LuPtBi [67–71,85] and the doped semiconductor $Sn_{1-x}In_xTe$ [86].

There is a close analogy between TIs and SCs in view of the Hamiltonian describing the systems. In particular, the Bogoliubov-de Gennes (BdG) Hamiltonian for the quasiparticles of a SC is similar to the Bloch Hamiltonian for a band insulator, where the superconducting gap corresponds to the band gap of the insulator. However, the Hamiltonian for TSC obeys the particle-hole symmetry which is not the case for TIs.

A time reversal invariant TSC possesses a full superconducting energy gap in the bulk but gapless surface states consisting of a single Majorana cone, which emerges for instance in the case of the ^{3}He-B phase. This class of SC is denoted by the $\mathbb{Z}_2$ invariant in 1D and 2D [75,87–89] and by the integer $\mathbb{Z}$ in 3D [75,88]. Based on the analogy between the Hamiltonians of a TRI superconductor and the QSHE, it has been argued that spin-up and spin-down electrons in the spin-triplet pairing channel form $p_x + ip_y$ and $p_x - ip_y$ Cooper pairs for a 2D TRI superconductor; *i.e.* the edge states of the system consist of spin-up and spin-down states with opposite chiralities [82]. As in the QSHE, these edge states are protected by TRS, and thus should be gapless and without any backscattering (see 3.2.2.1). In a 3D TRI superconductor, where both spin polarization and orbital angular momentum are vectors, the system is analogous to the case of the ^{3}He-B phase with a full pairing gap in the bulk. In contrast to 3D TIs, the surface states of the TSC may possibly host Majorana zero modes.

Along with time reversal invariant (TRI) TSCs, time reversal breaking (TRB) TSCs also attract tremendous interest as they give rise to non-Abelian statistics [90,91] and topological quantum computation, an active field of research [92]. Theoretically, a criterion for identification of topological phases in TRI and TRB superconductors has been proposed in details in Refs. [93–95].

3.3 Upper critical field B_{c2}

In a magnetic field superconductivity is suppressed. For a standard BCS SC this is predominantly due to two interactions of the magnetic field with the Cooper pairs (Werthamer, Helfand, Hohenberg-WHH model [96]):

(i) Interaction of the field with the orbital motion of the Cooper pairs (Lorentz force), which results in the orbital limit B_{c2}^{orb}.

(ii) Interaction of the field with the spins of the Cooper pairs (Zeeman effect), which results in the spin-pair breaking, or so-called paramagnetic limit B^P.

Overall, close to T_c the orbital depairing mechanism prevails, while the spin-pair breaking becomes dominant at low temperatures and in large fields.

According to the WHH approach, the orbital limiting upper critical field at 0 K depends simply on both T_c and the slope of $B_{c2}(T)$ at T_c

$$B_{c2}^{orb}(0) = \zeta T_c \left(dB_{c2} / dT \right)\Big|_{Tc}, \tag{3.9}$$

where the pre-factor ζ takes a value of 0.69 and 0.72 for the dirty (*i.e.* the mean free path $l \ll$ coherence length ξ) and clean limit (*i.e.* $l \gg \xi$), respectively [96].

The spin-pair breaking or Pauli limiting upper critical field is determined by a simple equation [97]

$$B^{P}(0) = 1.86 \times T_c . \tag{3.10}$$

In the presence of a magnetic field, the free energy of a SC changes. In particular, upon increasing the magnetic field, the free energy of the superconducting state increases, while in contrast the free energy of the normal state decreases. When these free energies become equal, the resulting upper-critical field can be defined

$$B_{c2}(0) = \frac{B_{c2}^{orb}(0)}{\sqrt{1+\alpha}}, \tag{3.11}$$

here α is a parameter that measure the relative strength of the orbital and spin-pair breaking effect. It is called the Maki parameter [98]

$$\alpha = \sqrt{2} B_{c2}^{orb}(0) / B^{P}(0). \tag{3.12}$$

Therefore, within the WHH formalism, the resulting $B_{c2}(0)$ depends sensitively on the magnitude of α, namely an increase of α would suppress $B_{c2}(0)$.

3.3.1 Slope of the upper critical field $B_{c2}(T)$

In the section above we have discussed the suppression of a SC in a magnetic field and showed a simple method to calculate the upper critical field B_{c2} for $T \to 0$. Furthermore, by studying the temperature dependence of the upper critical field $B_{c2}(T)$, which can be obtained by measuring the temperature dependence of the resistivity around the superconducting transition in fixed magnetic fields, we are able to obtain important information about the superconducting nature. In particular, the microscopic parameters of the superconducting state (*i.e.* the coherence length ξ) and the normal state (*i.e.* the mean free path ℓ) can be retrieved by employing the initial slope of the upper-critical field dB_{c2}/dT at T_c. This method is based on the Ginzburg-Landau theory for type-II superconductors under the assumption of a spherical

Fermi surface. This analysis has been applied to A15 compounds [99] and heavy fermion systems [100]. The slope of $B_{c2}(T)$ can be expressed by

$$B'_{c2} = -\left.\frac{\partial B_{c2}}{\partial T}\right|_{T_c} = R(l)\left(1.18\times10^{35}\frac{\gamma^2 T_c}{S_s^2} + 4480\gamma\rho_0\right) \qquad (3.13)$$

where S_s is the part of the Fermi surface where Cooper pairs are formed; the parameter R(ℓ) varies between R = 1 and R = 1.17 in the dirty and in the clean limit, respectively; γ is the Sommerfeld term in the electronic specific heat (per unit volume). Note that all parameters are in SI units. In the clean limit (ρ_0 small, $l \gg \xi$) the first term dominates B'_{c2}, whereas in the dirty limit (ρ_0 large, $l \ll \xi$) B'_{c2} is mainly determined by the second term. Subsequently, the microscopic parameters (*i.e.* ℓ, ξ) can be extracted

$$l = a\frac{1}{\rho_0 S_s},\ \xi = b\frac{S_s}{\gamma T_c}, \qquad (3.14)$$

where the quantities a and b are given by 1.533 × l0^6 Ω and 6.61 × l0^{-26} J/K, respectively.

3.3.2 Temperature variation of the upper critical field $B_{c2}(T)$

Strictly speaking, the classification of unconventional superconductivity based on the total spin S and orbital angular momentum L is not applicable in case of a material which has strong spin-orbit coupling such as a heavy fermion system [101]. Instead of a classification in singlet (S = 0) and triplet (S = 1) states, the total angular momentum J should be considered. However, it is not expected that the superconducting properties of such strong orbit-coupling systems are significantly different from the ones studied by using rather simple models ignoring spin-orbit coupling. To this purpose, two theoretical models have been chosen: the WHH [96] and polar state models [80], which can be considered representative for all possible pairing states.

The WHH model describes *s*-wave pairing in the clean and dirty limit of superconductors and is expressed by the following equation [96,102]

$$\ln\frac{1}{t} = \sum_{n=-\infty}^{n=+\infty}\left\{\frac{1}{|2n+1|} - \frac{\left(\frac{t}{\sqrt{h}}\right)J(\alpha_\omega)}{1-\left(\frac{\lambda}{\sqrt{h}}\right)J(\alpha_\omega)}\right\}, \qquad (3.15)$$

where $$J(\alpha_\omega) = 2\int_0^\infty d\omega \exp(-\omega^2)\tan^{-1}(\alpha_\omega\omega) \qquad (3.16)$$

and $\alpha_\omega = \dfrac{\sqrt{h}}{\left(|2n+1|t+\lambda\right)}$; $t = \dfrac{T}{T_c}$; $h = 2eB_{c2}\left(\dfrac{v_F}{2\pi T_c}\right)^2$; $\lambda = \dfrac{1}{2\pi T_c \tau} = 0.882\xi / l$; (3.17)

here, t is a reduced temperature with T_c the zero-field SC transition temperature and h is a reduced magnetic field. The reduced mean collision frequency λ is related to the coherence length ξ and the mean free path l and takes the value zero in the clean limit ($\xi \ll l$) and infinity in the dirty limit ($\xi \gg l$). Note that the $h(t)$ curve for the clean limit is above the one for the dirty limit case. In order to get an equal slope at t = 1 for all $h(t)$ curves the normalization frequently used is

$$h^*(t) \equiv \frac{B_{c2}}{\left(-dB_{c2}/dT\right)\big|_{T=T_c}} = \frac{h}{\left(-dh/dt\right)\big|_{t=1}}. \qquad (3.18)$$

The slope dh/dt varies as a function of λ [103,104]

$$\left(-dh/dt\right)\big|_{t=1} = 3\lambda^2\left[\left(\pi^2\lambda/4\right) - \psi\left(1/2 + 1/2\lambda\right) + \psi\left(1/2\right)\right]^{-1}, \qquad (3.19)$$

where ψ is the digamma function, which takes values from 1.426 for $\lambda = 0$ to 1.216λ for large λ [102].

In the second model, *p*-wave SC, using the normal state Green's function for a SC in a magnetic field and taking into account merely the polar state, *i.e.* the equal spin pairing state (ESP: $\left|\uparrow\uparrow\right\rangle$ and $\left|\downarrow\downarrow\right\rangle$), the temperature dependence of the upper-critical field is given by [80]

$$\ln t = \sum_{n=-\infty}^{n=+\infty}\left[s(\omega_n) - \frac{1}{|2n+1|}\right], \qquad (3.20)$$

with $$s(\omega_n) = 2\frac{t}{\sqrt{h}}\int_0^\infty du\, e^{-u^2}\left(\tfrac{3}{2}\{[1+(\alpha_\omega u)^{-2}]\tan^{-1}\alpha_\omega u - (\alpha_\omega u)^{-1}\}\right), \qquad (3.21)$$

$\alpha_w = \dfrac{\sqrt{h}}{t|2n+1|}$, the reduced temperature $t = \dfrac{T}{T_c}$ with T_c a zero-field SC transition temperature and a reduced magnetic field $h = 2eB_{c2}\left(\dfrac{v_F}{2\pi T_c}\right)^2$.

The solutions of equations (3.15) and (3.20) have been applied to the two candidates for TSCs $Cu_xBi_2Se_3$ [84] and YPtBi [67] presented in detail in the chapters 4 and 5, respectively.

References

[1] H. V. Löhneysen, A. Rosch, M. Vojta, and P. Wölfle, Rev. Mod. Phys. **79**, 1015 (2007).

[2] W. Young, Phys. B **91B**, 213 (1977).

[3] M. A. Continentino, G. M. Japiassu, and A. Troper, Phys. Rev. B. Condens. Matt. **39**, 9734 (1989).

[4] M. A. Ruderman and C. Kittel, Phys. Rev. **96**, 99 (1954).

[5] J. Kondo, Prog. Theor. Phys. **32**, 37 (1964).

[6] H. Löhneysen, T. Pietrus, G. Portisch, H. Schlager, A. Schröder, M. Sieck, and T. Trappmann, Phys. Rev. Lett. **72**, 3262 (1994).

[7] P. Gegenwart, F. Kromer, M. Lang, G. Sparn, C. Geibel, and F. Steglich, Phys. Rev. Lett. **82**, 1293 (1999).

[8] O. Trovarelli, C. Geibel, S. Mederle, C. Langhammer, F. M. Grosche, P. Gegenwart, M. Lang, G. Sparn, and F. Steglich, Phys. Rev. Lett. **85**, 626 (2000).

[9] J. Custers, P. Gegenwart, H. Wilhelm, K. Neumaier, Y. Tokiwa, O. Trovarelli, C. Geibel, F. Steglich, C. Pépin, and P. Coleman, Nature **424**, 524 (2003).

[10] S. A. Grigera, R. S. Perry, A. J. Schofield, M. Chiao, S. R. Julian, G. G. Lonzarich, S. I. Ikeda, Y. Maeno, A. J. Millis, and A. P. Mackenzie, Science **294**, 329 (2001).

[11] C. Pfleiderer, G. J. McMullan, S. R. Julian, and G. G. Lonzarich, Phys. Rev. B **55**, 8330 (1997).

[12] M. Uhlarz, C. Pfleiderer, and S. Hayden, Phys. Rev. Lett. **93**, 256404 (2004).

[13] P. Niklowitz, F. Beckers, G. Lonzarich, G. Knebel, B. Salce, J. Thomasson, N. Bernhoeft, D. Braithwaite, and J. Flouquet, Phys. Rev. B **72**, 024424 (2005).

[14] S. Drotziger, C. Pfleiderer, M. Uhlarz, H. Löhneysen, D. Souptel, W. Löser, and G. Behr, Phys. Rev. B **73**, 214413 (2006).

[15] H. V. Löhneysen, A. Schroder, T. Trappmann, and M. Welsch, J. Magn. Magn. Mater. **108**, 45 (1992).

[16] M. Nicklas, M. Brando, G. Knebel, F. Mayr, W. Trinkl, and A. Loidl, Phys. Rev. Lett. **82**, 4268 (1999).

[17] A. de Visser, M. J. Graf, P. Estrela, A. Amato, C. Baines, D. Andreica, F. N. Gygax, and A. Schenck, Phys. Rev. Lett. **85**, 3005 (2000).

[18] D. Sokolov, M. Aronson, W. Gannon, and Z. Fisk, Phys. Rev. Lett. **96**, 116404 (2006).

[19] R. Küchler, P. Gegenwart, J. Custers, O. Stockert, N. Caroca-Canales, C. Geibel, J. G. Sereni, and F. Steglich, Phys. Rev. Lett. **96**, 256403 (2006).

[20] J. Sereni, T. Westerkamp, R. Küchler, N. Caroca-Canales, P. Gegenwart, and C. Geibel, Phys. Rev. B **75**, 024432 (2007).

[21] H. K. Onnes, Leiden Comm. **120b, 122b**, **124c** (1911).

[22] J. Bardeen, L. N. Cooper, and J. R. Schrieffer, Phys. Rev. **108**, 1175 (1957).

[23] D. D. Osheroff, R. C. Richardson, and D. M. Lee, Phys. Rev. Lett. **28**, 885 (1972).

[24] A. J. Leggett, Rev. Mod. Phys. **47**, 331 (1975).

[25] F. Steglich, J. Aarts, C. D. Bredl, W. Lieke, D. Meschede, W. Franz, and H. Schafer, Phys. Rev. Lett. **43**, 1892 (1979).

[26] A. de Visser, J. J. M. Franse, A. Menovsky, and T. T. M. Palstra, J. Phys. F: Met. Phys. **14**, L191 (1984).

[27] W. Schlabitz, J. Baumann, B. Pollit, U. Rauchschwalbe, H. M. Mayer, U. Ahlheim, and C. D. Bredl, Z. Phys. B **62**, 171 (1986).

[28] R. Movshovich, T. Graf, D. Mandrus, J. D. Thompson, J. L. Smith, and Z. Fisk, Phys. Rev. B. Condens. Matt. **53**, 8241 (1996).

[29] N. D. Mathur, F. M. Grosche, S. R. Julian, I. R. Walker, D. M. Freye, R. K. W. Haselwimmer, and G. G. Lonzarich, Nature **394**, 39 (1998).

[30] S. S. Saxena, P. Agarwal, K. Ahilan, F. M. Grosche, R. K. W. Haselwimmer, M. J. Steiner, E. Pugh, I. R. Walker, S. R. Julian, P. Monthoux, G. G. Lonzarich, A. Huxley, I. Sheikin, D. Braithwaite, and J. Flouquet, Nature **406**, 587 (2000).

[31] D. Aoki, A. Huxley, E. Ressouche, D. Braithwaite, J. Flouquet, J. P. Brison, E. Lhotel, and C. Paulsen, Nature **413**, 613 (2001).

[32] J. D. Thompson, R. Movshovich, Z. Fisk, F. Bouquet, N. J. Curro, R. A. Fisher, P. C. Hammel, H. Hegger, M. F. Hundley, M. Jaime, P. G. Pagliuso, C. Petrovic, N. E. Phillips, and J. L. Sarrao, J. Magn. Magn. Mater. **226-230**, 5 (2001).

[33] E. Bauer, G. Hilscher, H. Michor, C. Paul, E. Scheidt, A. Gribanov, Y. Seropegin, H. Noël, M. Sigrist, and P. Rogl, Phys. Rev. Lett. **92**, 027003 (2004).

[34] H. Kamimura, H. Ushio, S. Matsuno, and T. Hamada, *Theory of Copper Oxide Superconductors* (Springer-Verlag, Berlin, 2005).

[35] J. G. Bednorz and K. A. Müller, Z. Phys. B **193**, 189 (1986).

[36] H. Hosono, J. Phys. Soc. Jpn. **77**, 1 (2008).

[37] J. A. Wilson, J. Phys. Condens. Matt. **22**, 203201 (2010).

[38] D. Fay and J. Appel, Phys. Rev. B **22**, 3173 (1980).

[39] A. Huxley, I. Sheikin, E. Ressouche, N. Kernavanois, D. Braithwaite, R. Calemczuk, and J. Flouquet, Phys. Rev. B **63**, 144519 (2001).

[40] F. Hardy, A. Huxley, J. Flouquet, B. Salce, G. Knebel, D. Braithwaite, D. Aoki, M. Uhlarz, and C. Pfleiderer, Phys. B Condens. Matt. **359-361**, 1111 (2005).

[41] T. Akazawa, H. Hidaka, T. Fujiwara, T. C. Kobayashi, E. Yamamoto, Y. Haga, R. Settai, and Y. Onuki, J. Phys. Condens. Matt. **16**, L29 (2004).

[42] A. Dommann, F. Hulliger, T. Siegrist, and P. Fischer, J. Magn. Magn. Mater. **67**, 323 (1987).

[43] S. Sakarya, W. Knafo, N. H. van Dijk, Y. Huang, K. Prokes, C.Meingast, and H. v. Löhneysen, J. Phys. Soc. Jpn. **79**, 014702 (2010).

[44] N. T. Huy, A. Gasparini, D. E. de Nijs, Y. Huang, J. C. P. Klaasse, T. Gortenmulder, A. de Visser, A. Hamann, T. Görlach, and H. v. Löhneysen, Phys. Rev. Lett. **99**, 067006 (2007).

[45] N. T. Huy, D. E. de Nijs, Y. Huang, and A. de Visser, Phys. Rev. Lett. **100**, 077002 (2008).

[46] E. Slooten, T. Naka, A. Gasparini, Y. Huang, and A. de Visser, Phys. Rev. Lett. **103**, 097003 (2009).

[47] V. P. Mineev and T. Champel, Phys. Rev. B **69**, 144521 (2004).

[48] D. Belitz and T. Kirkpatrick, Phys. Rev. B **69**, 184502 (2004).

[49] T. Kirkpatrick and D. Belitz, Phys. Rev. B **67**, 024515 (2003).

[50] R. Roussev and A. Millis, Phys. Rev. B **63**, 140504 (R) (2001).

[51] A. de Visser, N. T. Huy, A. Gasparini, D. E. de Nijs, D. Andreica, C. Baines, and A. Amato, Phys. Rev. Lett. **102**, 167003 (2009).

[52] T. Ohta, Y. Nakai, Y. Ihara, K. Ishida, K. Deguchi, N. K. Sato, and I. Satoh, J. Phys. Soc. Jpn. **77**, 023707 (2008).

[53] T. Ohta, T. Hattori, K. Ishida, Y. Nakai, E. Osaki, K. Deguchi, N. K. Sato, and I. Satoh, J. Phys. Soc. Jpn. **79**, 023707 (2010).

[54] S. Julian, Physics **5**, 17 (2012).

[55] V. P. Mineev and K. V. Samokhin, *Introduction to Unconventional Superconductivity* (Gordon and Breach Science Publishers, Amsterdam, 1999).

[56] V. P. Mineev, in *Adv. Theor. Phys. Landau Meml. Conf.* (2009), p. 68.

[57] V. P. Mineev, Phys. Rev. B **66**, 134504 (2002).

[58] C. L. Kane and E. J. Mele, Phys. Rev. Lett. **95**, 226801 (2005).

[59] M. König, S. Wiedmann, C. Brüne, A. Roth, H. Buhmann, L. W. Molenkamp, X.-L. Qi, and S.-C. Zhang, Science **318**, 766 (2007).

[60] M. Z. Hasan and C. L. Kane, Rev. Mod. Phys. **82**, 3045 (2010).

[61] D. V. Griffiths, *Introduction to Quantum Mechanics* (Prentice Hall, Inc., 1995), p. 333.

[62] D. Hsieh, Y. Xia, L. Wray, D. Qian, A. Pal, J. . H. Dil, J. Osterwalder, F. Meier, G. Bihlmayer, C. . L. Kane, Y. S. Hor, R. J. Cava, and M. Z. Hasan, Science **323**, 919 (2009).

[63] X.-L. Qi and S.-C. Zhang, Phys. Today **63**, 33 (2010).

[64] H. Zhang, C.-X. Liu, X.-L. Qi, X. Dai, Z. Fang, and S.-C. Zhang, Nat. Phys. **5**, 438 (2009).

[65] S. Chadov, X. Qi, J. Kübler, G. H. Fecher, C. Felser, and S. C. Zhang, Nat. Mater. **9**, 541 (2010).

[66] H. Lin, L. A. Wray, Y. Xia, S. Xu, S. Jia, R. J. Cava, A. Bansil, and M. Z. Hasan, Nat. Mater. **9**, 546 (2010).

[67] T. V. Bay, T. Naka, Y. K. Huang, and A. de Visser, Phys. Rev. B **86**, 064515 (2012).

[68] T. V. Bay, M. Jackson, C. Paulsen, C. Baines, A. Amato, T. Orvis, M. C. Aronson, Y. K. Huang, and A. de Visser, Solid State Commun. **183**, 13 (2014).

[69] G. Goll, M. Marz, A. Hamann, T. Tomanic, K. Grube, T. Yoshino, and T. Takabatake, Phys. B Condens. Matt. **403**, 1065 (2008).

[70] A. P. Schnyder, P. M. R. Brydon, and C. Timm, Phys. Rev. B **85**, 024522 (2012).

[71] F. F. Tafti, T. Fujii, A. Juneau-Fecteau, S. René de Cotret, N. Doiron-Leyraud, A. Asamitsu, and L. Taillefer, Phys. Rev. B **87**, 184504 (2013).

[72] Y. Pan, A. M. Nikitin, T. V. Bay, Y. K. Huang, C. Paulsen, B. H. Yan, and A. de Visser, Europhys. Lett. **104**, 27001 (2013).

[73] A. Altland and M. R. Zirnbauer, Phys. Rev. B **55**, 1142 (1997).

[74] M. Sigrist and K. Ueda, Rev. Sci. Instrum. **63**, 239 (1991).

[75] A. Kitaev, AIP Conf. Proc. **1134**, 22 (2009).

[76] A. P. Mackenzie and Y. Maeno, Rev. Mod. Phys. **75**, 657 (2003).

[77] P. W. Anderson and P. Morel, Phys. Rev. **123**, 1911 (1961).

[78] R. Balian and N. R. Werthamer, Phys. Rev. **131**, 1553 (1963).

[79] T. Tsuneto, *Superconductivity and Superfluidity* (Cambridge University Press, New York, 2005).

[80] K. Scharnberg and R. Klemm, Phys. Rev. B **22**, 5233 (1980).

[81] S.-Q. Shen, *Topological Insulators-Dirac Equation in Condensed Matters* (Springer, Berlin, 2012).

[82] X.-L. Qi and S.-C. Zhang, Rev. Mod. Phys. **83**, 1057 (2011).

[83] Y. S. Hor, A. J. Williams, J. G. Checkelsky, P. Roushan, J. Seo, Q. Xu, H. W. Zandbergen, A. Yazdani, N. P. Ong, and R. J. Cava, Phys. Rev. Lett. **104**, 057001 (2010).

[84] T. V. Bay, T. Naka, Y. K. Huang, H. Luigjes, M. S. Golden, and A. de Visser, Phys. Rev. Lett. **108**, 057001 (2012).

[85] N. P. Butch, P. Syers, K. Kirshenbaum, A. P. Hope, and J. Paglione, Phys. Rev. B **84**, 220504 (R) (2011).

[86] S. Sasaki, Z. Ren, A. A. Taskin, K. Segawa, L. Fu, and Y. Ando, Phys. Rev. Lett. **109**, 217004 (2012).

[87] R. Roy, ArXiv:0803.2868v1 (2008).

[88] A. Schnyder, S. Ryu, A. Furusaki, and A. Ludwig, Phys. Rev. B **78**, 195125 (2008).

[89] X.-L. Qi, T. Hughes, S. Raghu, and S.-C. Zhang, Phys. Rev. Lett. **102**, 187001 (2009).

[90] N. Read and D. Green, Phys. Rev. B **61**, 10267 (2000).

[91] D. A. Ivanov, Phys. Rev. Lett. **86**, 268 (2001).

[92] C. Nayak, A. Stern, M. Freedman, and S. Das Sarma, Rev. Mod. Phys. **80**, 1083 (2008).

[93] M. Sato, Phys. Rev. B **81**, 220504(R) (2010).

[94] M. Sato, Phys. Rev. B **79**, 214526 (2009).

[95] L. Fu and E. Berg, Phys. Rev. Lett. **105**, 097001 (2010).

[96] N. R. Werthamer, E. Helfand, and P. C. Hohenberg, Phys. Rev. **147**, 295 (1966).

[97] A. M. Clogston, Phys. Rev. Lett. **9**, 266 (1962).

[98] K. Maki, Phys. Rev. **148**, 362 (1966).

[99] T. P. Orlando, E. J. J. McNiff, S. Foner, and M. R. Beasley, Phys. Rev. B **19**, 4545 (1979).

[100] A. de Visser, PhD Thesis, University of Amsterdam, 1986.

[101] U. Rauchschwalbe, Phys. **147B** 1 (1987).

[102] E. Helfand and N. R. Werthamer, Phys. Rev. **147**, 288 (1966).

[103] L. P. Gor'kov and Z. Eksperim, Sov. Phys. JETP **9**, 1364 (1959).

[104] L. P. Gor'kov and Z. Eksperim, Sov. Phys. JETP **10**, 998 (1960).